Influence of virtual surfaces on Frank elastic constants in a polymer-stabilized bent-core nematic liquid crystal

P. Lakshmi Madhuri, Uma S. Hiremath, C. V. Yelamaggad, K. Priya Madhuri, and S. Krishna Prasad
Centre for Nano and Soft Matter Sciences, Jalahalli, Bangalore 560013, India
(Received 3 December 2015; published 18 April 2016)

Effect of a polymer network on the threshold voltage of the Fréedericksz transition, Frank elastic constants, switching speed, and the rotational viscosity are investigated in a polymer-stabilized bent-core nematic liquid crystal with different polymer concentrations. These polymer networks form virtual surfaces with a finite anchoring energy. The studies bring out several differences in comparison to similar studies with a calamitic liquid crystal as the nematic host. For example, on varying the polymer content the threshold voltage decreases initially, but exhibits a drastic increase above a critical concentration. A similar feature—reaching a minimum before rising—is seen for the bend elastic constant, which gets enhanced by an order of magnitude for a polymer content of 2.5 wt %. In contrast, the splay elastic constant has a monotonic variation although the overall enhancement is comparable to that of the bend elastic constant. The behavior changing at a critical concentration is also seen for the switching time and the associated rotational viscosity. The presence of the polymer also induces a shape change in the thermal dependence of the bend elastic constant. We explain the features observed here on the basis of images obtained from the optical and atomic force microscopy.

DOI: 10.1103/PhysRevE.93.042706

I. INTRODUCTION

Polymer-stabilized liquid crystals (PSLCs) have attracted significant attention in recent times owing to their potential applications in memory effects [1] and electro-optic devices [1,2]. They are fabricated through *in situ* polymerization of reactive molecules dissolved in a conventional low molar mass LC. This network of polymer strands formed as a consequence of polymerization provides virtual surfaces in the bulk of the cell sandwiching the sample. These virtual surfaces play two important roles: (i) Confinement of the liquid crystal and imposing restriction on the length scale available to the self-assembled structure and (ii) present a surface anchoring force that supports or opposes the anchoring at the substrate surface. A point to be emphasized is that the network stabilizes the liquid crystal director configuration present at the time of its formation. A number of studies exist in the literature reporting the influence of the polymer network on liquid crystals. There have been studies on blue phases [3,4], ferroelectric smectic-C^* [5–10], and antiferroelectric smectic-C^*_A phases [11,12], but those on nematic LC [13] have received far more attention (for a recent review, see Ref. [2]). Applications which have been addressed include displays [14], light shutters, switchable windows [15], and photonic devices [16]. For example, blue phases stabilized by the polymer exhibit wide viewing angle and fast response times [17], features desirable for displays. The networks also influence the dielectric relaxation modes [18], alter the Fréedericksz threshold voltage and improve the switching-off dynamics in a device [19], and control photoconductivity [20]. All these studies involve only calamitic/discotic liquid crystals, whereas the recently revived class of bent-core liquid crystals (BLCs) [21] in a polymer-stabilized environment has hardly been investigated [22].

Liquid crystals formed of bent-core molecules, although known for more than a century, have come to the forefront only in recent times [21]. The reduced symmetry of these molecules, vis-à-vis their rodlike counterparts, results in phases with structures that have no analogy in the latter class. For example, even with achiral molecules ferroelectric or antiferroelectric polar ordering is obtained. In contrast, the bent-core nematic phase (BCN) is a rarity unlike in calamitic systems [23]. Interestingly, BCNs exhibit certain extraordinary properties. For example, Fréedericksz-transition data show that the splay elastic constant K_{11} has comparable values in the calamitic as well bent-core systems; the bend elastic constant K_{33} is one order of magnitude smaller. Further, K_{11} is almost always much higher than K_{33} [24–29], except on approach to a smectic phase, if it exists. Dictated by the energy cost of the associated director (average orientation direction of the molecules) deformation, the elastic constants influence the threshold and steepness of the electro-optic response, thus governing the performance of display devices. Apart from this practical necessity to understand the elastic behavior, the determination of the elastic constants also is used as a powerful tool to test the theoretical predictions, especially in the framework of mean-field models.

In this paper we describe the influence of a superimposed polymer-stabilized network on the splay and bend Frank elastic constants of a BCN compound. The electric Fréedericksz-transition method has been employed to determine the elastic constants. The results show that the low and high network density regimes have contrasting behavior not only in the magnitude of the elastic constants but their temperature dependence also. The switch-off time and the associated rotational viscosity also show network density-dependent behavior, getting lowered for high network densities. Some of these observations are at variance with those observed for PSLC systems with rodlike nematic host [19]. The morphology of the network as imaged by polarizing optical microscopy and atomic force microscopy are considered in interpreting the data.

II. EXPERIMENT

The BCN compound, 4-cyanoresorcinol bis[4-(4-*n*-hexyloxybenzoyloxy)benzoate] (6OCN for short), exhibits the

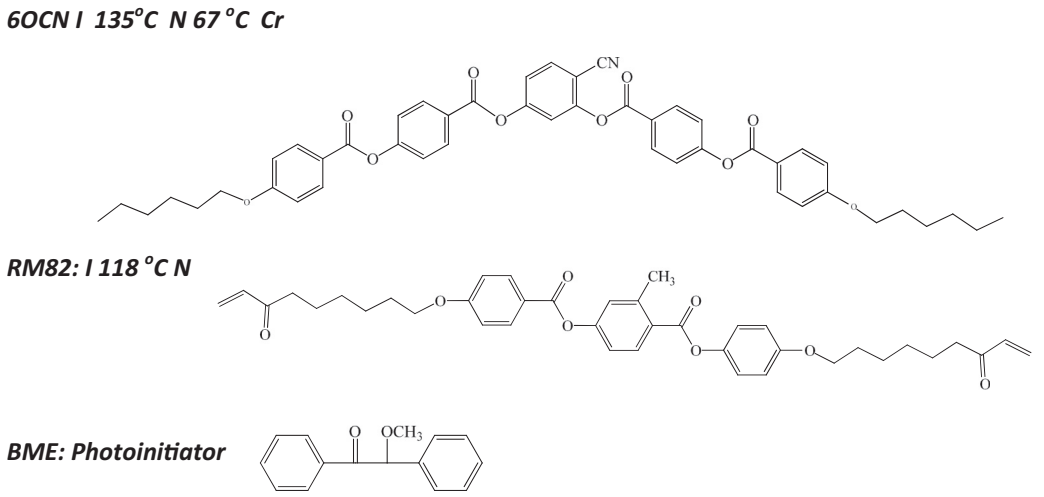

FIG. 1. Chemical structures and transition temperatures of the components employed.

nematic phase with a T_{NI} (nematic-isotropic transition temperature) of 135 °C, with a substantial supercooling [30,28]. For achieving the polymer stabilization of the host BLC, a photopolymerizable monomer, RM82 (from E. Merck) was used. This monomer is a diacrylated reactive compound, and being also a liquid crystal, helps in a homogeneous mixture of the two components. The polymerization of RM82 was facilitated by the addition of a small quantity (2% of the RM82 content) of a photoinitiator (BME, Aldrich). The transition temperatures of 6OCN and RM82 along with their chemical structures are shown in Fig. 1; the structure of BME is also given.

Experiments were conducted on pure 6OCN and seven polymer-stabilized BLC (PSBLC) mixtures spanning the range $X = 0.12$ to 2.5, where X indicates the composition of RM82 (by weight percent) in the mixture. The samples were sandwiched in cells (Awat, Poland) made of two indium tin oxide (ITO) -coated glass plates with an interplate gap of 9 μm; the inner surfaces of the plates were pretreated with a polymer layer and unidirectionally rubbed to achieve uniform planar orientation of the LC molecules. The samples were polymerized by employing a low power UV lamp with a peak wavelength of 365 nm: The intensity of UV light, measured using a UV power meter kept at the sample position, was 2 mW/cm^2. For the determination of the splay (K_{11}) and bend (K_{33}) elastic moduli, we probed the material permittivity through the electric field driven Fréedericksz transition. Owing to the positive dielectric anisotropy ε_a ($=\varepsilon_{\parallel}-\varepsilon_{\perp}$, where $\parallel$ and $\perp$ indicate the probing directions parallel, and perpendicular to, the nematic director **n**, respectively) of the sample at the probing frequency of 1 kHz. In the geometry employed, an electric field applied normal to the substrate plane results in a positive torque on **n** causing reorientation of the molecules towards the homeotropic orientation well above a certain threshold voltage, V_{th}. This results in the permittivity changing from $\varepsilon_{\perp}$ for $V < V_{th}$ to $\varepsilon_{\parallel}$ for $V \gg V_{th}$. Measurements of permittivity were done with a precision LCR meter (Agilent 4890A) capable of applying an ac voltage up to 20 V. For certain higher concentration mixtures, a higher voltage was required to attain saturation of the sample response. For this purpose, the ALC apparatus from Instec Corp., USA was used and voltages up to 40 V were applied. Optical microscopy observations were done with a research-grade polarizing optical microscope (Leica DMRXP) fitted with a hybrid camera (Optonics, USA). An atomic force microscope (AFM) was also employed to look at the morphology of the polymer strands. For this purpose, after polymerization and the network formation, one of the glass plates was carefully removed. The other plate along with LC and the network was immersed in a container having acetone, and left undisturbed overnight. This process removed the LC completely, but left the polymer network intact on the glass plate, which was imaged using AFM. The imaging done at room temperature used an Agilent 5500 AFM in the noncontact mode employing a rectangular-shaped silicon probe (NSC-15 from MikroMasch, USA) with a resonance frequency of 325 kHz, a force constant of 46 N/m, and a nominal tip radius <20 nm. All the images were acquired under ambient conditions with a scanning speed of 1 line/s and analyzed using PICOVIEW software from Agilent.

III. RESULTS AND DISCUSSION

A simplified schematic of the cell geometry showing the polymer bundles and the LC molecules, along with the views in the field-off and field-on conditions drawn as per the scenario described in the literature, are presented in Fig. 2. The polymer bundles are shown to be like solid objects, but in reality, with lateral sizes (diameter for a perfect circular cross section) in the submicrometer range (as will be discussed later), the bundles would have trapped a sizable ($\sim$1000) LC molecules along the cross section. Also to be noted is that polymers are depicted to remain along the equilibrium orientational direction in the substrate plane even when the LC molecules (at least the nontrapped ones) are reoriented normal to the substrate plane by the applied electric field.

A. Dielectric constant

The employed procedure to determine the elastic constants relies on measuring the permittivity of the medium. Figure 3 presents the permittivity at a fixed frequency (1 kHz) of planar

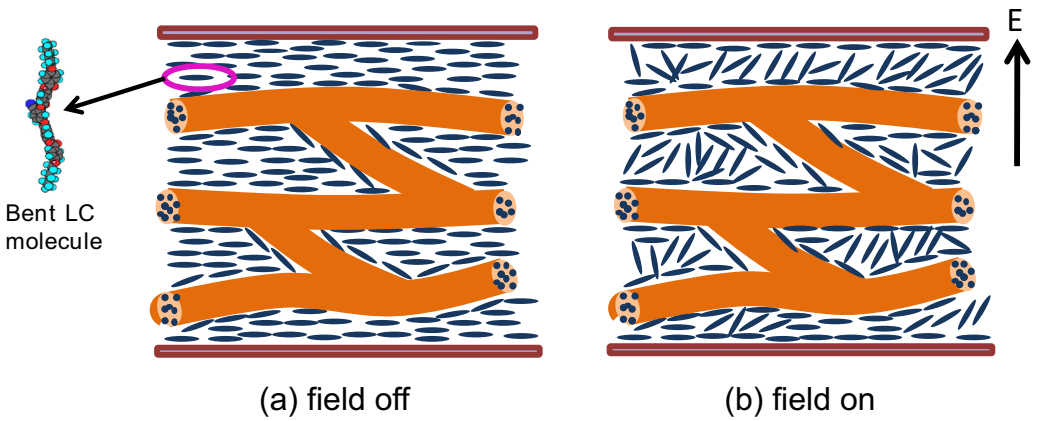

FIG. 2. Schematic of the cell geometry showing the polymer bundles and the LC molecules, in the (a) field-off and (b) field-on conditions. Polymers remain in the direction of the substrate plane even when the LC molecules (at least the nontrapped ones) are reoriented normal to the substrate plane by the applied electric field. The bundles have trapped a sizable (∼1000) LC molecules along the cross section.

oriented samples after polymerization; for the purpose of presentation the data for the different samples are normalized with respect to ε_{NI}, the value at T_{NI}, the isotropic-nematic transition temperature. The diminution in T_{NI} is essentially linear upon adding the polymer content; for the $X = 2.5$ mixture, the value reduces by 1.5 °C. Concomitantly $\delta\varepsilon = (\varepsilon_{NI}-\varepsilon_{\perp})$ also diminishes; here $\varepsilon_{\perp}$ is taken at a reduced temperature of $\Delta T = T_{NI}-6$ K (see inset to Fig. 3). This is due to the fact that the LC molecules get trapped between the polymer strands. For a sufficient concentration of the polymer, such a trapping can yield confinement effects on the LC sample. The finite dimension between the enclosing

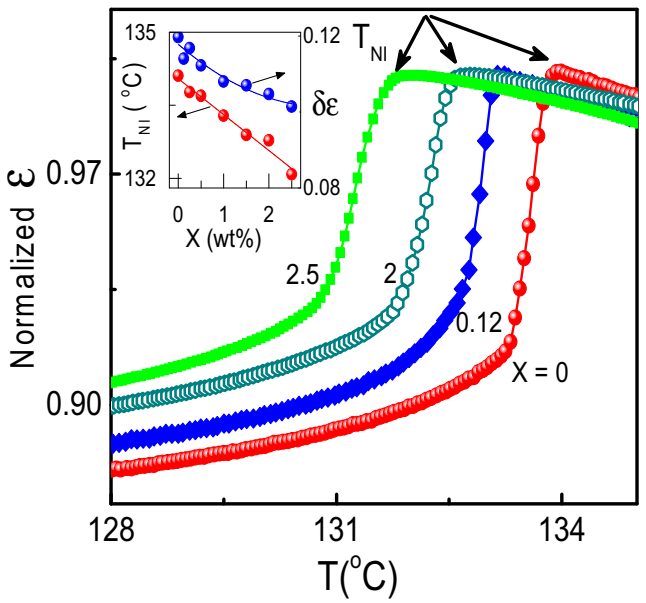

FIG. 3. Temperature dependence of permittivity in the planar configuration at 1 kHz for pure 6OCN ($X = 0$) and representative polymer-stabilized mixtures (concentrations of the polymer indicated against each curve). For the purpose of better presentation the data are normalized with respect to ε_{NI}, the value at the isotropic-nematic transition temperature (T_{NI}). Inset: Polymer stabilization is seen to lower T_{NI} as well as $\delta\varepsilon$, the difference in permittivity at T_{NI} and $\varepsilon_{\perp}$ in the nematic at a reduced temperature of $\Delta T = T_{NI}-6$ K.

polymer strands can restrict the extent of correlation of the phase structure of the LC material and reduce the magnitude of the order parameter resulting in a transition to the isotropic phase at a lower temperature. It should be noted that $\delta\varepsilon$, which can be taken to be a measure of the nematic order parameter, reduces by about 16% between the $X = 0$ and $X = 2.5$ mixtures. Considering the fact that the host molecule, 6OCN, has a strong CN dipole (dipole moment: 4.2 D) at the *ortho* position, reducing its concentration in the mixture would result in lowering of the dipole moment/unit volume (μ) of the system. This could account for the decrease in $\delta\varepsilon$. However, concentration-dependent change in μ can be expected to be ∼2.5% between the $X = 0$ and $X = 2.5$ mixtures. In contrast, $\delta\varepsilon$ reduces by 16%, suggesting that the change, over and above that dictated by μ, is due to diminution of the order parameter caused by the confinement.

B. Determination of elastic constants

1. Background

For quantitative determination of the elastic constants, we employed the one-dimensional theory [31]. Under the conditions that the sample has a positive ε_a, and the molecules are oriented in a planar fashion with the field being applied normal to the substrate plane, K_{11} is directly related to V_{th} by

$$K_{11} = \frac{\varepsilon_o \varepsilon_a V_{th}^2}{\pi^2}, \tag{1}$$

where ε_o is the permittivity of free space. The bend elastic constant K_{33} was determined from the full profile analysis, wherein the capacitance $C(V)$ dependence on voltage above V_{th} is described by

$$\frac{C(V)-C_{\perp}}{C_{\perp}} = \gamma - \frac{2\gamma}{\pi}\frac{V_{th}}{V}(1+\gamma\sin^2\phi_m)^{1/2} \times \int_0^{\phi_m}\left[\frac{(1+\kappa\sin^2\phi)(1-\sin^2\phi)}{(1+\gamma\sin^2\phi)(\sin^2\phi_m-\sin^2\phi)}\right]^{1/2}\cos\phi d\phi. \tag{2}$$

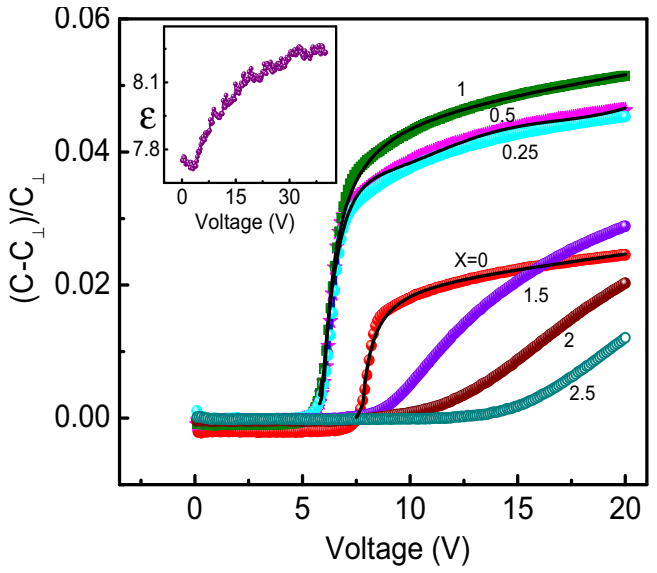

FIG. 4. Raw profiles of reduced capacitance with voltage at $\Delta T = 20$ K for the pure LC and the different mixtures. The numbers against the data sets indicate the concentration of RM82. Inset shows a raw profile taken with the ALC apparatus for $X = 1.5$ concentration mixture. The lines through the data for $X = 0$, 0.5, and 1 represent the fitting to Eq. (2).

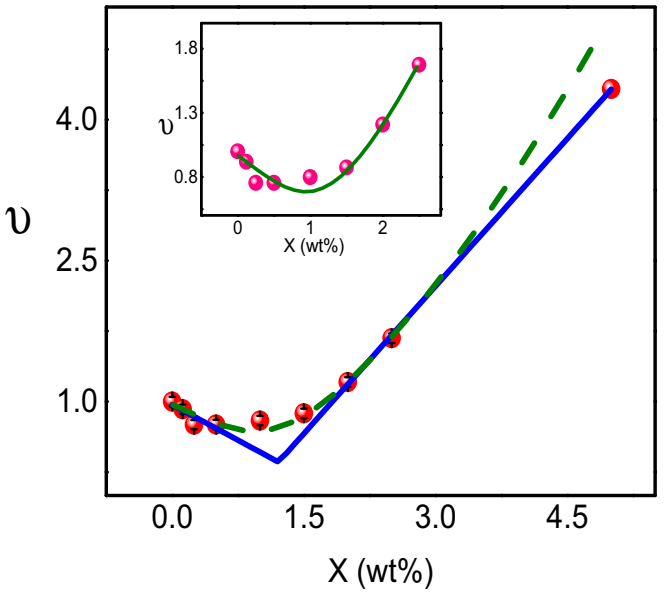

FIG. 5. Concentration dependence of the reduced threshold voltage $v = V_{\rm th}/V_{\rm o}$, where $V_{\rm th}$ and $V_{\rm o}$ are the Fréedericksz threshold voltage for, respectively, the corresponding polymer composite and pure 6OCN at the same ΔT. The value shows a lowering until a critical concentration $X_c = 0.9$, and then rapidly rises. The solid line represents a fit to Eq. (3) and the dashed line, a fit to Eq. (6).

Here $\kappa = K_{33}/K_{11}-1$, $\gamma = \varepsilon_{\rm a}/\varepsilon_{\perp}$, and ϕ is the angle between the director and the walls of the substrate with $\phi_{\rm m}$ being the value in the midplane of the sample; $\varepsilon_{\parallel}$ and $\varepsilon_{\perp}$ are obtained from the capacitance values $C_{\parallel}$ and $C_{\perp}$ measured parallel and perpendicular to the director. An iterative procedure written in MATLAB was used to obtain κ (and hence K_{33}) using γ and K_{11} as additional inputs. From the obtained κ, K_{33} can be calculated.

2. *Behavior of threshold voltage*

Raw profiles of the voltage dependence of the reduced capacitance $\Delta C = (C–C_{\perp})/C_{\perp}$ at a fixed $\Delta T = 20$ K are given in Fig. 4 for the pure compound and a few mixtures. Several features are seen to be influenced by polymer stabilization: (i) The content of RM82 alters $V_{\rm th}$ significantly, but in a nontrivial manner. For example, for the mixtures, $X = 0.25$, 0.5, and 1, $V_{\rm th}$ is lower than that for pure 6OCN. It, however, increases for concentrations $X > 1$. (ii) Up to $X \sim 1$, the system exhibits complete reorientation with ΔC achieving near saturation at high voltages. With further increase in the RM82 component, the reorientation becomes poorer and definitely incomplete even for the highest voltage applied. (iii) The rate at which ΔC increases above $V_{\rm th}$ is also affected by the extent of polymer stabilization, being sharper for $0 < X \leqslant 1$, but quite gradual for the higher concentrations. It was stated above that the diminution in T_{NI} and $\delta\varepsilon$ point to lowering of the order parameter with increasing X. But in the raw profiles of Fig. 4 it is seen that for $0 < X < 1$, the high-field limit of $\varepsilon(=\varepsilon_{\parallel})$ is higher than for pure 6OCN. If the order parameter were to determine $\varepsilon_{\parallel}$, this should not be the case. A possible explanation could be the following. Pure RM82 is weakly negative anisotropic (∼–0.9) material having a lower dielectric constant (∼5) than 6OCN. Being a minority component its influence on the anisotropy is still less as the system retains its positive anisotropy, a feature that could be judged from the Fréedericksz reorientation. Owing to the anchoring of the molecules at the polymer strands, the angle that the CN dipole at the *ortho* position makes with respect to the probing direction is slightly diminished. As we shall see below, for $X < 1$, the polymer strands would be short, and thus mobile. Thus the 6OCN molecules attached to the polymer strands still contribute to $\varepsilon_{\parallel}$ obtained through switching. The CN dipole of these molecules at the polymer surface is better oriented along the probing direction and consequently $\varepsilon_{\parallel}$ increases. The lines through the data points for $X = 0$, 0.5, and 1 represent fit to Eq. (2). As $X > 1$, the reduction of order parameter becomes dominant diminishing this effect. Further, the 6OCN molecules at the polymer surface do not participate in the switching process. Consequently $\varepsilon_{\parallel}$ reduces. The features (i)–(iii) mentioned above clearly point to the fact that polymer stabilization has a strong influence on both the splay and bend Frank elastic constants. It must be emphasized that while the last of the features mentioned is known for PSLC systems of rodlike nematics [19,32], $V_{\rm th}$ diminishing in the low concentration range is not reported.

Concentration dependence of normalized threshold voltage given by the ratio $v = V_{\rm th}/V_{\rm o}$, where $V_{\rm th}$ and $V_{\rm o}$ are the Fréedericksz threshold voltage for, respectively, the corresponding polymer composite and pure 6OCN at the same ΔT, is shown in Fig. 5. Thew striking feature is the nonmonotonic variation of the parameter: The value decreases up to $X \sim 1$, then reverses the trend getting doubled for $X = 2.5$. Assuming a linear trend in both the low and high concentration regions

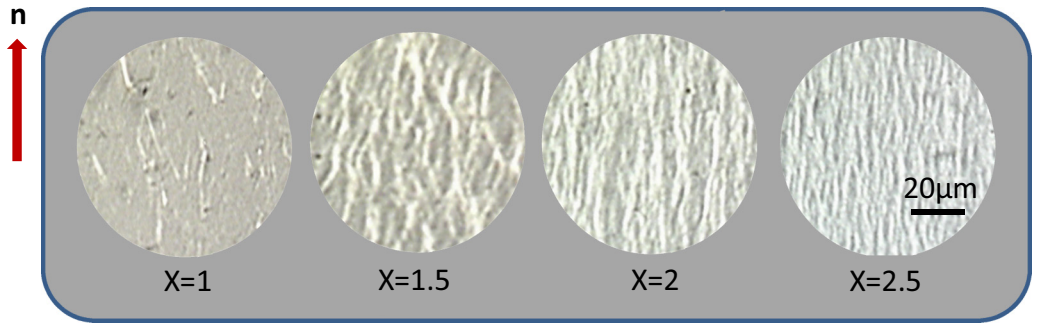

FIG. 6. Polarizing optical microscopy images taken in the isotropic phase of the mixture with concentrations $X = 1$, 1.5, 2, and 2.5. While the polymer fibrils are well developed for the latter three materials, the $X = 1$ mixture exhibits a few stray fibrils. It may also be noted in all the cases the fibrils are along the director direction (indicated by the arrow) of the host nematic. The network is seen to become denser with increasing concentration of RM82.

we fit the data to

$$v = A^{\pm} + X_c. \tag{3}$$

Here A^+ and A^- are the amplitudes in the high and low concentration regions, respectively. Obviously, the slope on the higher concentration side is much higher. The value of X_c, obtained as 0.9 ± 0.1, is the critical concentration at which the feature of V_{th} decreasing with X reverses the trend. To find out whether this surprising behavior is related to the formation of the polymer fibrils of RM82 molecules, we carried out polarizing microscopy studies on four mixtures on either side of X_c. To avoid the birefringence of the nematic phase dominating the field of view, the images were taken in the isotropic phase with a slight uncrossing of the microscope polarizers. The images obtained for the concentration $X = 1$, 1.5, 2, and 2.5 are shown in Fig. 6. The fibrils are quite well defined for $X > 1.5$ mixtures, their packing density increasing with X. In contrast, the $X = 1$ mixture shows a few sporadically placed fibrils. In fact for the PSBLC mixtures with $X < 1$ a few short strands are seen. Atomic force microscopy (AFM) images obtained on the $X = 1.5$ and 2 mixtures, presented in Fig. 7, support these observations, especially the increase of packing density of fibrils with increasing X [33]. The AFM images also show that the fibril diameter, which is 0.2 μm for the $X = 1.5$ mixture, increases to 0.6 μm for the $X = 2$ mixture. The increased packing density of the fibrils would enhance the restricted geometry effects on the confined nematic leading to an increased V_{th}. Such a feature is known for PSLC systems consisting of entirely rodlike LC molecules [19,32]. Further, the average density between the fibrils is given to be proportional to $1/X^2$. Thus the threshold field should have a quadratic dependence on X. With this in the background, we fitted in the entire range of X studied to $v \propto X^2$. The fitting, also shown in Fig. 5, is generally good except for the fact that it ignores V_{th} decreasing with X in the $X \leqslant 1$ region. As

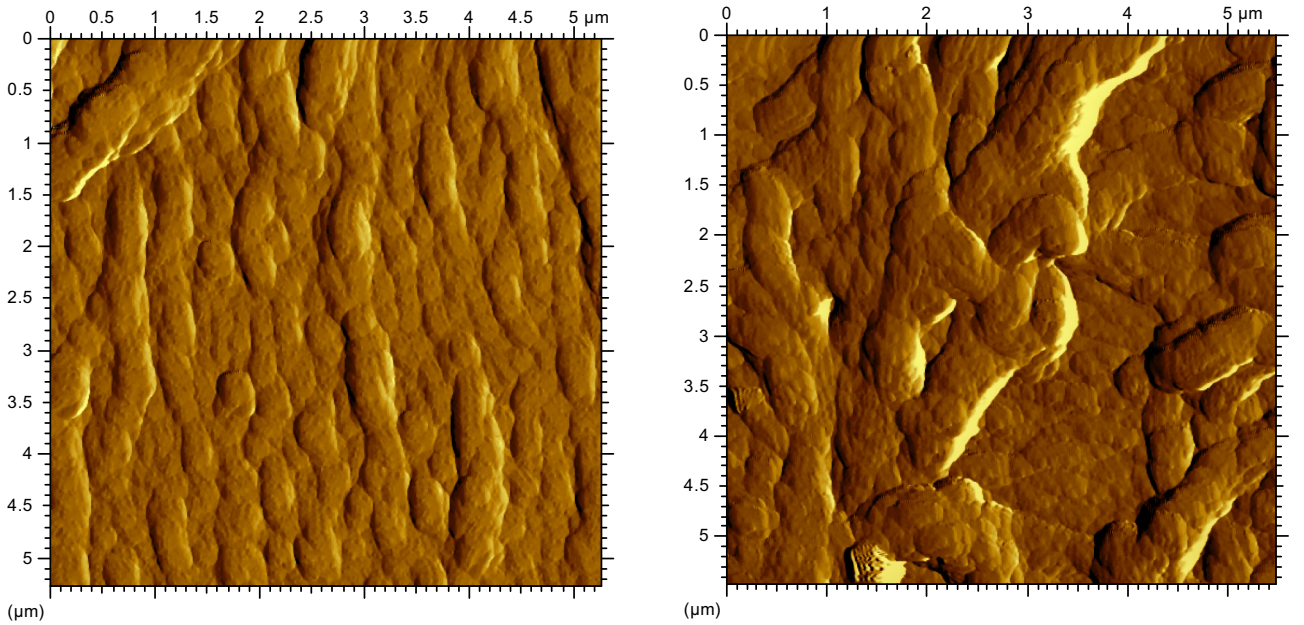

FIG. 7. AFM images of the $X = 1.5$ (left panel) and $X = 2$ (right panel) mixtures exhibiting well developed polymer strands. The diameter of the strands is more for the higher concentration mixture. The twisting of the strands seen in both the images is a surprising feature since neither the host nematic nor the polymerizing monomer is chiral in nature.

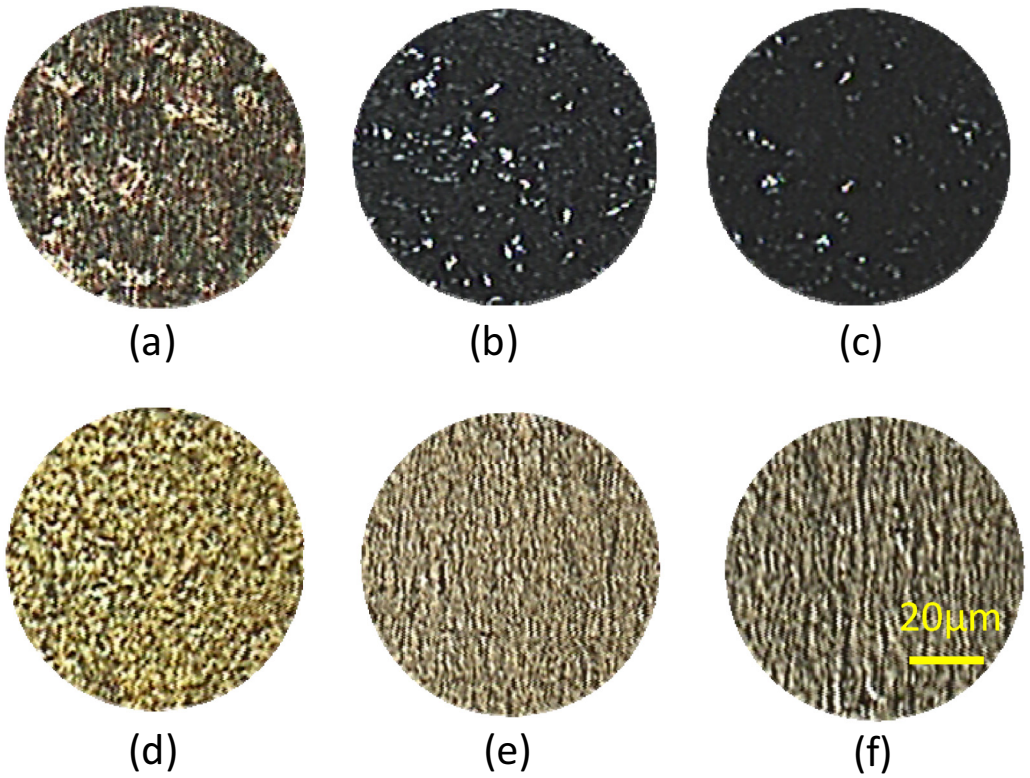

FIG. 8. POM images in the nematic phase of the $X = 1$ (top images) and $X = 2$ (bottom images) mixtures (a,d) in the absence of, and upon application of electric field with (b,e) 20 V and (c,f) 60 V magnitude, respectively. For $X = 1$, the reorientation of the host molecules drives the polymer strands also to reorient resulting in essentially a dark field of view. In contrast for the higher concentration mixture even at the highest field applied, the reorientation of the host molecules is not strong enough to reorient the polymer strands resulting in the field of view looking quite similar to the image in the isotropic phase (without any field), shown in Fig. 6.

noted earlier for $X \leqslant 1$ the fibrils are not formed properly, with a few short strands floating around. The short length of the fibrils perhaps helps in a better *mutual* interaction between the LC molecules and the strands. This would cause the strands also to switch their orientation to be generally parallel to the nematic director when the Fréedericksz transformation takes place. This is evident from the Polarising optical microscopy (POM) images taken with and without applied voltage for the $X = 1$ mixture [see Figs. 8(a)–8(c)]; compare especially images [Fig. 6(a)] taken in the isotropic phase clearly showing the fibrils, and Figs. 8(b) and 8(c) in the nematic switched state, which hardly show the fibrils since they would be end-on to the viewing direction. On the other hand, for the $X = 2$ mixture, even well beyond $V_{\rm th}$, the fibrils remain parallel to the surface [Figs. 8(d)–8(f)]. The better mutual influence between the strands and the LC molecules is responsible for the lowering of $V_{\rm th}$ for the mixtures in the subcritical region.

C. Theoretical model

In fact it has been argued by Kossyrev *et al.* [19] that the polymer fibrils create *virtual surfaces* with a finite anchoring energy throughout the bulk of the sample. These authors considered the diameter of the fibrils and the distance between them, parametrized in terms of a characteristic length ξ, to control this anchoring energy, and presented an expression wherein the critical field $E_{\rm th}$ is strongly dependent on ξ; obviously ξ becomes dependent on the density of the polymer fibrils. We now briefly recall this theory.

The starting point of the theoretical model [19], schematically shown in Fig. 9, is that the density of the polymer fibrils

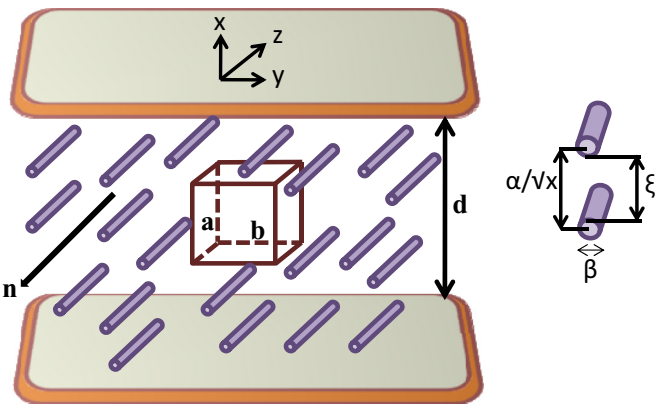

FIG. 9. Polymer fibrils aligned parallel to the nematic director **n** that is along the z axis in the absence of the electric field. The fibrils are assumed to be perfectly straight and the director domains bounded by rectangles of dimensions a and b. For saturating electric field, **n** reorients to point along the x axis. The average distance between the centers of the polymer fibrils depends on the concentration as $\alpha/\sqrt{X}$. The diameter of a fibril is β and the characteristic length is ξ (adapted from Ref. [19]).

(approximately the number of polymer fibrils per unit volume) is proportional to the concentration of the polymer. The fibrils are assumed to be perfectly straight, limiting the problem to two dimensions, described by the rectangle bounded by a and b. Consider the xyz coordinate system shown in Fig. 9. In the absence of the electric field the director $\mathbf{n}$, parallel to the fibrils, is along the z axis. For the saturating electric field $\mathbf{n}$ reorients to point along the x axis. The dimensions of the rectangle, a and b, are along x and y, respectively. The Fréedericksz transition in the cell with an electrode separation (cell thickness) of d occurs in each of these identical rectangles. The total free energy density (per unit volume) within each rectangular domain is given by

$$f_v = \frac{K}{2}\left[\left(\frac{\partial\theta}{\partial x}\right)^2 + \left(\frac{\partial\theta}{\partial y}\right)^2 - \frac{\varepsilon_a\varepsilon_0 E^2}{K}\sin^2\theta\right]. \quad (4)$$

Here $\theta\,(x, y)$ is the distortion angle of the nematic director with respect to the z axis. For strong anchoring boundary conditions at the surface of the director domain the free energy yields the critical electric field $E_{\rm th}$,

$$E_{\rm th} = \sqrt{\frac{\Pi^2 K}{\varepsilon_a\varepsilon_0}\left[\left(\frac{1}{a}\right)^2 + \left(\frac{1}{b}\right)^2\right]}. \quad (5)$$

The average distance between the randomly distributed fibrils of diameter β is concentration dependent and represented by the characteristic length $\xi = \alpha/\sqrt{X} - \beta$. Considering finite surface anchoring at the rectangular director domains, the energy W of which is taken to be of the Rapini-Papoular form, the critical electric field $E_{\rm th}$ is given by

$$E_{\rm th} \cong \sqrt{\frac{\Pi^2 K}{\varepsilon_a\varepsilon_0}\left[\left(\frac{1}{d} + \frac{1}{\xi + 2K/W}\right)^2 + \left(\frac{1}{\xi + 2K/W}\right)^2\right]}. \quad (6)$$

The data shown in Fig. 5 were fit to Eq. (6). The fitting is seen to be good (see Fig. 5) except that the $X = 5$ data yield α and β values to be 2.7 and 0.2 μm, respectively. It may be noted that the β value is in very good agreement with the diameter of the fibrils seen from the AFM images. The fitting also suggests that ξ, the characteristic length which represents the distance between fibrils, decreases from 7.6 to 1.5 μm as the concentration changes from $X = 0.12$ to 2.5, pointing to the fact that the packing density of the fibrils increases with polymer content. For $X = 1.5$, the anchoring energy is found to be 4.4×10^{-6} J/m^2, a value comparable to the typical anchoring energies. The most interesting aspect of this comparison with the theoretical model is that the nonmonotonic character of the threshold voltage is reflected in the theory also.

D. Behavior of elastic constants

The temperature dependences of splay and bend elastic constants, K_{11} and K_{33} for pure 6OCN and the PSBLC samples, are shown in Figs. 10 and 11. Computation of K_{11} and K_{33} through Eqs. (1) and (2) requires the parameters $\varepsilon_\perp$, $\varepsilon_\parallel$, and ε_a. For pure 6OCN as well as $X < X_c$ mixtures we obtained $\varepsilon_\perp$ and $\varepsilon_\parallel$ from the low ($V < V_{\rm th}$) and the high ($V > V_{\rm th}$)

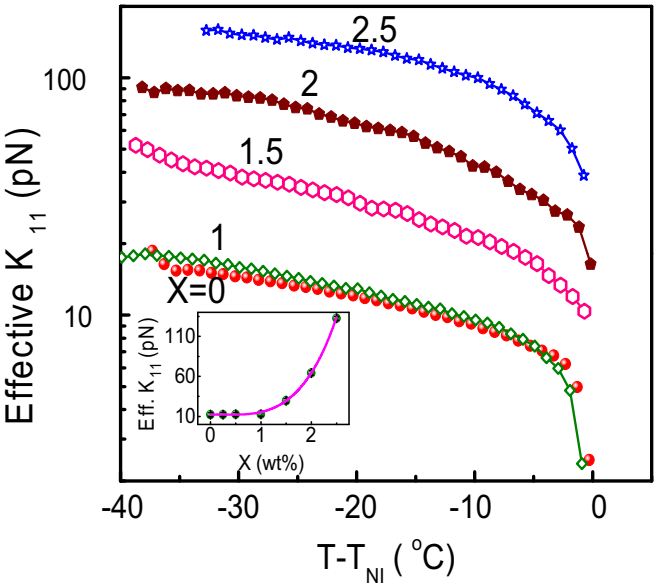

FIG. 10. Temperature dependence of the splay elastic constant K_{11} for pure 6OCN and a few mixtures, whose concentration is indicated against each curve. In all cases the thermal dependence is monotonic. The magnitude of K_{11} increases by more than an order of magnitude over the concentration range $X = 0$ to 2.5, as seen from the data taken at a reduced temperature of $\Delta T = 20$ K, presented in the inset.

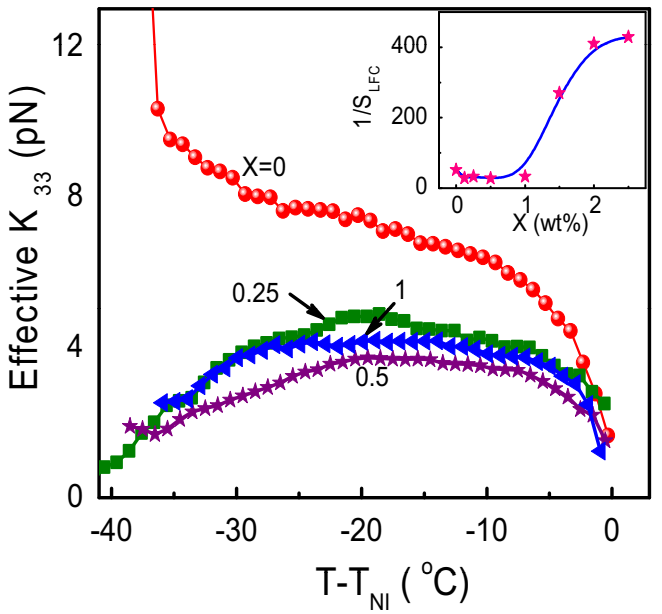

FIG. 11. Thermal variation of the bend elastic constant K_{33} for pure 6OCN and the mixtures in the concentration regime (concentration X is indicated against each curve). While pure 6OCN ($X = 0$) has a monotonic variation, the mixtures have a convex-shaped profile. The strong increase in the value for pure 6OCN at low temperatures is due to the development of smectic correlations. The inset shows the reciprocal of the slope $S_{\rm LFC}$ of the capacitance vs voltage curves (such as those presented in Fig. 4) in the region immediately above $V_{\rm th}$, taken at a reduced temperature of $\Delta T = 20$ K. This parameter is considered as a measure of K_{33} over the entire concentration range studied, and exhibits a drastic increase.

voltage region, respectively, of the capacitance-dependent voltage profiles, such as those shown in Fig. 4. While the former parameter was obtained directly, $\varepsilon_\parallel$ was calculated by plotting ΔC vs the reciprocal of the applied voltage $(1/V)$ and extrapolating the fitted straight line to $1/V = 0$. The calculation was straightforward over this concentration range since ΔC tends towards saturation for 20 V, the highest voltage that could be obtained with the LCR meter. This was not true for $X > X_c$ mixtures. Therefore, for these materials we determined $\varepsilon_\parallel$ using the ALC apparatus by increasing the applied voltage up to 40 V; even this range was not sufficient for the $X = 5$ mixture. It may also be noted that the signal to noise ratio of the data from the ALC apparatus was not of the same quality as those from the LCR meter (a typical profile of the voltage-dependent permittivity for $X = 1.5$ is shown in the inset of Fig. 4). Therefore the ALC data were used only getting ε_a, but not for the determination of K_{33}. Another point to be noted here is the following. Previous investigations on calamitic systems argue that the consideration $V_{\rm th} = E_{\rm th} d$, wherein d is the cell thickness, is strictly valid only for the bulk system, and for the polymer-stabilized materials d should be taken as the interfibrillar distance. Further, the elastic constants are argued to be unaltered from those for the pure LC, and the K values obtained from Eqs. (1) and (2) would be effective values. Taking the interfibrillar distance to substitute for cell thickness d and using $V_{\rm th} = E_{\rm th}\, d$, we can write $K_{11f} \propto \frac{\varepsilon_a V_{{\rm th}f}^2 d_f^2}{d^2}$, where the subscript f indicates the values for the mixtures with the polymer fibers present. From AFM images the interfibrillar distance for $X = 2$ appears to be of the order of 0.6 microns. Now, if K_{11} remains unaltered ($K_{11f} = K_{11}$ for a pure sample) then $V_{{\rm th}f}$ for the mixture should increase by a factor of 7.5 (with ε_a being higher by a factor of 2 for the mixture), whereas experiments indicate a much smaller increase of 1.2 times. Thus we prefer to use the cell thickness for the calculation. Hence the elastic constant values obtained for PSBLC samples, to be described below, are effective ones. With these caveats let us look at the temperature dependence of K_{11} and K_{33}. Firstly, the relative magnitude of the elastic constants satisfying the relation $K_{11} > K_{33}$, known [24,28,29] for the host 6OCN compound, is seen in other PSBLC samples. The molecular shape (of the host BLC) with a bent contour has been reasoned [27,34] to favor bend deformation of the director causing K_{33} to be lower than K_{11}, the opposite of which being generally true for calamitic materials [35]. This could mean that for all the materials studied here, the bent-core component is dominating the elastic behavior. For further interpretation, we consider two regions: region I having $X \leqslant X_c$ and region II with $X > X_c$. As noted from microscopy images, discussed earlier, in region I, the polymer strands of RM82 molecules are hardly formed, but well developed in region II. Thus in the former region we may consider the material, for argument's sake, to be nonpolymeric. Also to be noted is the experimental feature that in region I, ε_a and thus K_{33} are properly determined. It is interesting to note that in this region while K_{11} is essentially unaltered, K_{33} gets nearly halved for the mixtures. Since concentration of the bent-core component 6OCN gets reduced as X increases, this is a surprising result. If any reduction in the order parameter is the cause for the decrease in K_{33} a similar trend must have been true for K_{11} as well. In the light of a concentration-independent K_{11}, we would like to recall a feature of K_{33} reported for mixtures consisting of bent-core and rodlike materials [26–29,34]. More often than not such mixtures exhibit a convex-shaped profile for the temperature dependence of K_{33}, rarely seen for pure bent-core compounds, and never for calamitic materials. We have previously argued [29] that the frustration set in by the shape difference of the molecules is responsible for the convex shape. As already discussed, in region I of the presently studied system the polymer strands are yet to be formed properly, and the interaction between the 6OCN and RM82 molecules would still be on molecular length scales. Thus any frustration between the bent 6OCN and the rodlike RM82 can lead to the behavior seen in Fig. 11.

In region II polymerization leads to well developed polymer strands which confine the LC molecules. This region exhibits a significant increase in K_{11}, the value, in comparison for pure 6OCN, an order of magnitude larger for the $X = 2.5$ mixture, and it should be, in principle, much higher for the $X = 5$ mixture. Such large values in K_{11} are indeed reported for nematic materials made of polymeric mesogens. For example, Zheng-Min and Kléman [36] have reported for a polyester with a degree of polymerization of 25, splay elastic constant values of 300 pN. The theoretical model of de Gennes also expects very high values of K_{11} for polymeric systems, and predicts that K_{11} scales as L^2, the square of the polymer length. Whether the small concentration of the RM82 molecules with the long polymer fibrils can achieve this in the present composite system is a topic for further deliberation.

As mentioned earlier owing to the nonsaturation of the capacitance, Eq. (2) cannot be used to calculate K_{33} properly for the higher concentration mixtures. However, to get a measure of the bend elastic constant, we consider the following. The slope $S_{\rm LFC}$ of the reduced capacitance vs applied voltage profile in the region immediately above $V_{\rm th}$ is expected to be a measure of K_{33}. Specifically [37],

$$\kappa_{\rm LFC} = \gamma\left(\frac{2}{S_{\rm LFC}} - 1\right) - 1. \tag{7}$$

Here $\kappa_{\rm LFC} = K_{33}/K_{11} - 1$. But Eq. (4), although it appears to be simple method to get K_{33}, has problems since the range of the validity of linearization is not clear. This could lead to erroneous values especially if there is an inflection point near $V_{\rm th}$. It may, however, be noted that with increasing X, the slope of the capacitance vs voltage (Fig. 4) profile decreases. Thus, we presume that the problems associated with the simplifications of Eq. (4) may not be serious, but still present the reciprocal of $S_{\rm LFC}$ as a measure of K_{33}. Such data are presented in the inset of Fig. 11. A huge increase in this parameter is seen with increasing X suggesting that the bend deformation also is less favored once the polymer fibrils are properly formed.

E. Dynamics of switching

To obtain the dynamic character of the Fréedericksz switching, we measured the time decay of the sample capacitance

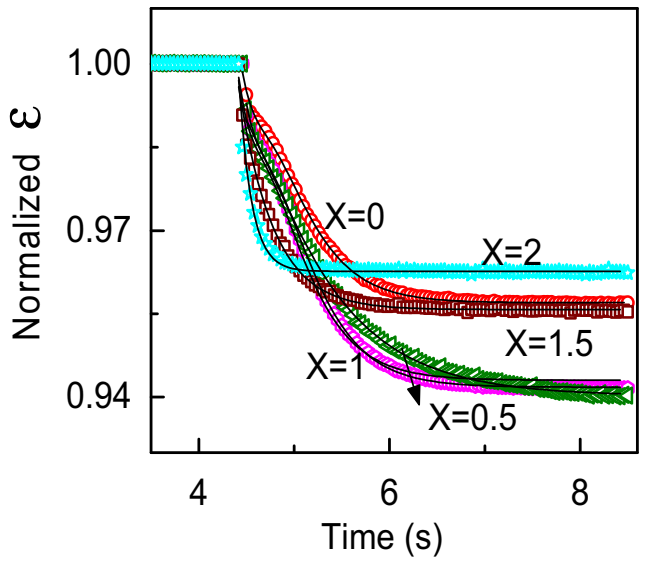

FIG. 12. Transient capacitance response when the applied voltage is abruptly removed at a reduced temperature of $\Delta T = 5$ K for 6OCN ($X = 0$) and different mixtures; the data are normalized with respect to the zero-time value for 6OCN. The higher ($X > 1$) concentration mixtures show a single relaxation, whereas the materials with $X \leqslant 1$ have two relaxations. The lines through the data for 6OCN and $X = 2$ represent fits to Eqs. (10) and (8), respectively.

followed by the application of a step voltage to the sample at a frequency of 1 kHz. A high data rate LCR meter (Agilent 4980) with suitable computer interfacing was employed to collect time-dependent capacitance values. The method involves application of an ac voltage ($V > V_{\text{th}}$) to the planar oriented sample and abruptly lowering to a value $V \ll V_{\text{th}}$ initiating the nematic director to relax to the initial planar configuration, while simultaneously recording the change in the effective cell capacitance. In the small signal regime, δC, the difference between the capacitance (C_t) at an instant t and the equilibrium capacitance ($C_\perp$) is governed by the simple exponential decay expression

$$\delta C = \delta C_o[\exp(-2t/\tau_{\text{off}})]. \tag{8}$$

Using the calculated relaxation time τ_{off} and K_{11}, the rotational viscosity γ_1 can be determined by

$$\gamma_1 = \frac{\tau_{\text{off}} K_{11} \pi^2}{d^2}. \tag{9}$$

The raw transient capacitance profiles are shown for pure 6OCN and a few PSBLC mixtures. It is interesting to see that while 6OCN and $X < X_c$ mixtures exhibit a two-step relaxation [38], the higher concentration $X = 1.5$ and 2 mixtures present a single process (Fig. 12). While the single process was analyzed using Eq. (8), the transient two-step data were analyzed with the help of a sum of two exponential functions,

$$C(t) = A_0 + \frac{A_1}{\left\{1 + \exp\left(\frac{-t}{\tau_1}\right)\right\}} + \frac{A_2}{\left\{1 + \exp\left[\frac{-(t-A_3)}{\tau_2}\right]\right\}}, \tag{10}$$

where A_0 to A_3 are fit parameters, and τ_1 and τ_2 are the relaxation times associated with the two relaxation processes. Here we consider τ_{off} to be equal to τ_2.

Figures 13(a) and 13(b) present the thermal variation (in terms of reciprocal temperature) of τ_{off} and γ_1 for 6OCN and the mixtures; for reasons already stated the viscosity values for the mixtures are to be considered as effective. On the semilogarithmic scale employed, both parameters exhibit an essentially linear variation over the temperature range studied indicating that the associated process is Arrhenius and governed by activation energy w. Using the standard Arrhenius expression, w was determined from the γ_1 data and is in the range of 80 ± 9 kJ/mol for the different materials. The inset of Fig. 13(a) presents the τ_{off} values at a fixed reduced temperature of $\Delta T = 5$ K bringing out the interesting feature that τ_{off} decreases with increasing X, but after reaching a maximum in the region of the critical concentration X_c. It is interesting to know that the model of Kossyrev *et al.* [19] also predicts that $\tau_{\text{off}} \propto \frac{1}{E_{\text{th}}^2}$. Since E_{th} goes to a minimum near

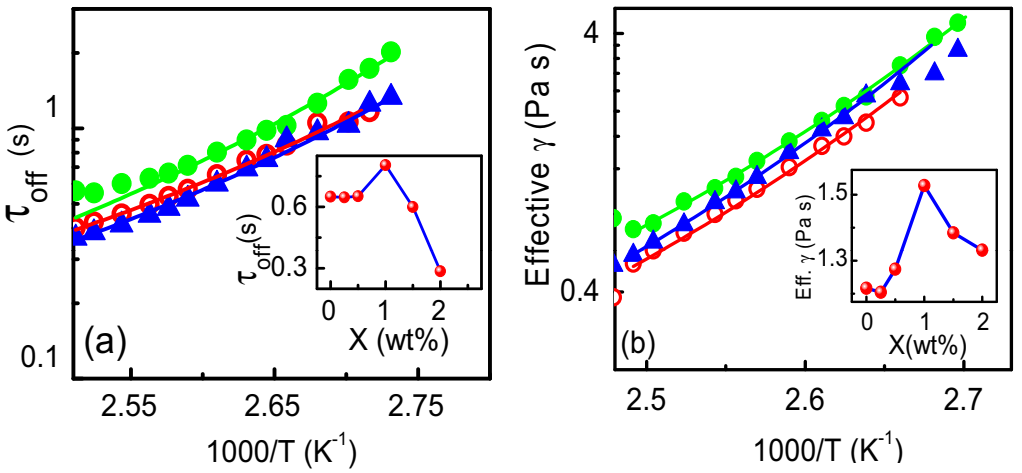

FIG. 13. Semilogarithmic representation of the inverse temperature dependence of (a) τ_{off} and (b) the associated rotational viscosity for representative materials (open circle: $X = 0$, filled circle: $X = 1$, and triangle: $X = 1.5$) studied. The essentially linear variation of both the parameters in such a representation suggests Arrhenius behavior. Both parameters exhibit a nonmonotonic dependence on the concentration of RM82, with a maximum at $X \sim 1$, as seen from the insets.

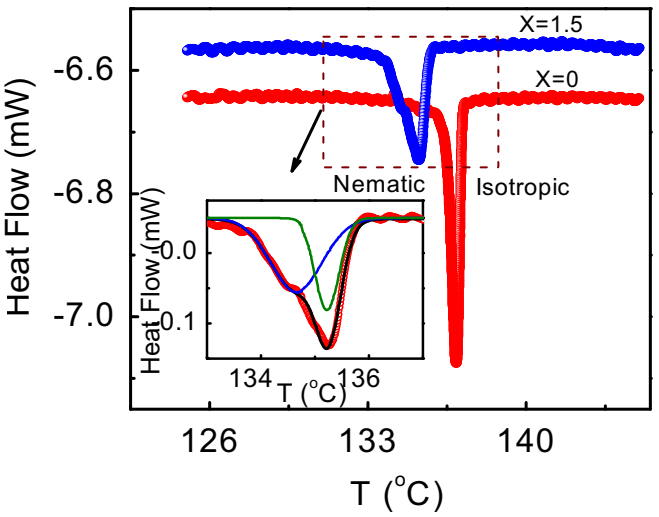

FIG. 14. Differential scanning calorimetric profiles in the vicinity of the isotropic-nematic transition for pure 6OCN and the mixture $X = 1.5$. While the former exhibits a single sharp peak, the profile for the mixture showing a shoulder can be resolved into two peaks, as depicted on an enlarged scale in the inset. The lower temperature peak is connected with the transition occurring for molecules in the vicinity of the polymer strands. Also to be noted is that although the peak height is greatly reduced for the mixture, the peak area, corresponding to the enthalpy of the transition, is comparable for the two materials.

X_c(Fig. 5) τ_{off} should have a maximum, as indeed seen from the inset to Fig. 13(a). This further supports the agreement between the theoretical model and the present experiments. The parameter A_3 in Eq. (10) is the delay before the second exponent takes over the dynamics of relaxation; A_3 decreases with X. Thus it can be concluded that the polymer fibril formation influences the switching dynamics also both in terms of the relaxation time as well as the delay time.

F. Differential scanning calorimetry

Finally, we discuss an interesting aspect observed in differential scanning calorimetric scans for a PSBLC mixture with a concentration slightly higher than X_c. Figure 14 presents the scan obtained in the vicinity of the isotropic-nematic transition for the mixture. For comparison the scan for pure 6OCN is also provided. While the pure compound exhibits a sharp single peak, the mixture has a much weaker and broader thermal signature, with a shoulder at lower temperatures. Fitting the profile to a sum of two Gaussians, we can resolve the two peaks (see inset of Fig. 14). Since POM observations do not show any noticeable changes at the second temperature, we attribute it to the I-N transition occurring for the molecules at the surface of the polymer strands. Such surface transitions are known in cases where the restricted geometry plays an important role, e.g., in nanocolloidal aerosol and LC systems [39,40]. The fact that the total enthalpy is comparable to that for pure 6OCN and that the enthalpies of the individual peaks are comparable suggests that a large number of molecules are influenced by the polymer strands.

IV. CONCLUSIONS

The influence of polymer stabilization on the Fréedericksz transition in a bent-core nematic has been investigated and the splay and bend Frank elastic constants have been extracted. These studies on bent-core nematics show that the threshold voltage has a nonmonotonic dependence with polymer concentration: It diminishes initially but increases drastically after reaching a minimum at a critical concentration. Such a feature has not been reported for polymer-stabilized nematics. The splay elastic constant K_{11} varies monotonically with polymer concentration, and increases by an order of magnitude when the polymer content reaches 2.5 wt %. Over the same concentration range the bend elastic constant also appears to get enhanced by an order of magnitude. However, K_{33} exhibits a lowering in the value for small polymer concentrations. Further, K_{11} has a monotonic variation with temperature for the pure compound as well as for the mixtures. In contrast the thermal variation of K_{33} is monotonic for the pure compound, but has a convex-shaped profile for the polymer-stabilized samples. Optical as well as atomic force microscopy studies bring out the aspect that for concentrations below the critical value the polymer is present as short strands, whereas above it, well developed long fibrils exist. We provide an explanation for the lowering of V_{th} on the basis of this feature. For the field-off situation, the Fréedericksz dynamic switching profiles exhibit two relaxation profiles for pure 6OCN and low concentration PSBLC samples. Increasing the polymer content results in a single relaxation process. Concomitantly, the relaxation time gets halved for high polymer content; the value becomes highest for the critical concentration mixture, however. Both switching time and the extracted rotational viscosity have a temperature dependence which can be explained by an Arrhenius expression with comparable activation energy for the different materials studied. The studies bring out several differences in comparison to the behavior of polymer-stabilized samples with rodlike host compounds. Investigation with different chemical architectures of the bent-core compounds are required before concluding whether the differences observed between the rodlike and bent-core materials are generic.

ACKNOWLEDGMENTS

The authors are thankful to Dr. Neena Susan John, Centre for Nano and Soft Matter Sciences, Bangalore, for the permission to use the Atomic Force Microscope apparatus. They also thank Mr. Y. Venkata Jayasurya, TIFR (India), Mumbai for his valuable help in MATLAB programming.

[1] R. Blinc, I. Musevic, J. Pirs, M. Skarabot, and B. Zeks, in *Liquid Crystals in Complex Geometries*, edited by G. P. Crawford and S. Zumer (Taylor and Francis, London, 1996); D. J. Broer, G. P. Crawford, and S. Zumer, *Cross-Linked Liquid Crystalline Systems* (CRC Press, Boca Raton, FL, 2011).

[2] I. Dierking, Polym. Chem. **1**, 1153 (2010).

[3] H. Kikuchi, M. Yokota, Y. Hisakado, H. Yang, and T. Kajiyama, Nat. Mater. **1**, 64 (2002); H. Kikuchi, S. Izena, H. Higuchi, Y. Okumura, and K. Higashiguchi, Soft Matter **11**, 4572 (2015).

[4] D. Xu, J. Yan, J. Yuan, F. Peng, Y. Chen, and S.-T. Wu, Appl. Phys. Lett. **105**, 011119 (2014).

[5] R. A. M. Hikmet and M. Michielsen, Adv. Mater. **7**, 300 (1995).

[6] M. Petit, J. Hemine, A. Daoudi, M. Ismaili, J. M. Buisine, and A. Da Costa, Phys. Rev. E **79**, 031705 (2009).

[7] C. A. Guymon, L. A. Dougan, P. J. Martens, N. A. Clark, D. M. Walba, and C. N. Bowman, Chem. Mater. **10**, 2378 (1998).

[8] P. Archer, I. Dierking, and M. A. Osipov, Phys. Rev. E **78**, 051703 (2008); S. Kaur, I. Dierking, and H. F. Gleeson, Eur. Phys. J. E **30**, 265 (2009).

[9] I. Dierking, Materials **7**, 3568 (2014).

[10] L. M. Blinov, E. P. Pozhidaev, F. V. Podgornov, S. A. Pikin, S. P. Palto, A. Sinha, A. Yasuda, S. Hashimoto, and W. Haase, Phys. Rev. E **66**, 021701 (2002).

[11] J. Strauss and H.-S. Kitzerow, Appl. Phys. Lett. **69**, 725 (1996); P. Rudquist, D. Elfstroem, S. T. Lagerwall, and R. Dabrowski, Ferroelectrics **344**, 177 (2006); H. Furue and H. Yokoyama, Jpn. J. Appl. Phys. **42**, 6180 (2003).

[12] P. L. Madhuri, S. K. Prasad, and G. G. Nair, RSC Adv. **4**, 3121 (2014).

[13] See, e.g., R. A. M. Hikmet, Adv. Mater. **4**, 679 (1992); Y. K. Fung, A. Borstnik, S. Zumer, D.-K. Yang, and J. W. Doane, Phys. Rev. E **55**, 1637 (1997); D.-K. Yang, L.-C. Chien, and J. W. Doane, Appl. Phys. Lett. **60**, 3102 (1992).

[14] D. K. Yang, in *Progress in Liquid Crystal Science and Technology: In Honor of Shunsuke Kobayashi's 80th Birthday*, edited by H. Kwok, S. Naemura, and H. L. Ong, Series on Liquid Crystals Vol. 4 (World Scientific, Singapore, 2013).

[15] J. Pirš, M. Olenik, B. Marin, S. Žumer, and J. W. Doane, J. Appl. Phys. **68**, 3826 (1990).

[16] V. Jayalakshmi, G. Hegde, G. G. Nair, and S. K. Prasad, Phys. Chem. Chem. Phys. **11**, 6450 (2009).

[17] G. Nordendorf, A. Hoischen, J. Schmidtke, D. Wilkes, and H.-S. Kitzerow, Polym. Adv. Technol. **25**, 1195 (2014).

[18] See, e.g., *Broadband Dielectric Spectroscopy*, edited by F. Kremer and A. Schonhals (Springer, Berlin, 2003).

[19] P. A. Kossyrev, J. Qi, N. V. Priezjev, R. A. Pelcovits, and G. P. Crawford, Appl. Phys. Lett. **81**, 2986 (2002).

[20] S. K. Prasad, G. G. Nair, G. Hegde, U. S. Hiremath, and C. V. Yelamaggad, Liq. Cryst. **31**, 1265 (2004).

[21] A. Ramamurthy, *Thermotropic Liquid Crystals: Recent Advances* (Springer, Berlin, 2007).

[22] B. Atorf, A. Hoischen, M. B. Ros, N. Gimeno, C. Tschierske, G. Dantlgraber, and H. Kitzerow, Appl. Phys. Lett. **100**, 223301 (2012).

[23] A. Jakli, Liq. Cryst. Rev. **1**, 65 (2013).

[24] K. S. Krishnamurthy, P. Tadapatri, and W. Weissflog, Soft Matter **7**, 6273 (2011).

[25] M. Majumdar, P. Salamon, A. Jakli, J. T. Gleeson, and S. Sprunt, Phys. Rev. E **83**, 031701 (2011).

[26] P. Sathyanarayana, B. K. Sadashiva, and S. Dhara, Soft Matter **7**, 8556 (2011).

[27] B. Kundu, R. Pratibha, and N. V. Madhusudana, Phys. Rev. Lett. **99**, 247802 (2007).

[28] S. K. Prasad, P. L. Madhuri, U. S. Hiremath, and C. V. Yelamaggad, Appl. Phys. Lett. **104**, 111906 (2014).

[29] P. L. Madhuri, S. K. Prasad, U. S. Hiremath, and C. V. Yelamaggad, Appl. Phys. Lett. **104**, 241111 (2014); S. Parthasarathi, D. S. Shankar Rao, K. Fodor Csorba, and S. K. Prasad, J. Phys. Chem. B **118**, 14526 (2014).

[30] L. Kovalenko, M. W. Schröder, R. A. Reddy, S. Diele, G. Pelzl, and W. Weissflog, Liq. Cryst. **32**, 857 (2005).

[31] H. Gruler, J. Chem. Phys. **61**, 5408 (1974); T. Uchida and Y. Takahashi, Mol. Cryst. Liq. Cryst., Lett. Sect. **72**, 133 (1981).

[32] R.-Q. Ma and D.-K. Yang, Phys. Rev. E **61**, 1567 (2000).

[33] It may be noted that the AFM image for $X = 2$ exhibits twisted strands, although neither of the components involved (RM82 and 6OCN) are chiral in nature. It is possible that the inherent chirality associated with the bent shape of the bent-core molecules, known to impart chirality in ordered smectic phases, is responsible for the twist of the fibrils. However, this may not have a direct bearing on the results discussed here.

[34] P. Sathyanarayana, M. Mathew, Q. Li, V. S. S. Sastry, B. Kundu, K. V. Le, H. Takezoe, and S. Dhara, Phys. Rev. E **81**, 010702 (2010).

[35] G. Vertogen and W. H. de Jeu, in *Thermotropic Liquid Crystals, Fundamentals*, Springer Series in Chemical Physics Vol. 45 (Springer-Verlag, Berlin, 1988), p. 104.

[36] S. Zheng-Min and M. Kléman, Mol. Cryst. Liq. Cryst. **111**, 321 (1984).

[37] S. W. Morris, P. Palffy-Muhoray, and D. A. Balzarini, Mol. Cryst. Liq. Cryst. **139**, 263 (1986).

[38] P. Tadapatri, U. S. Hiremath, C. V. Yelamaggad, and K. S. Krishnamurthy, J. Phys. Chem. B **114**, 1745 (2010).

[39] M. Caggioni, A. Roshi, S. Barjami, F. Mantegazza, G. S. Iannacchione, and T. Bellini, Phys. Rev. Lett. **93**, 127801 (2004).

[40] V. Jayalakshmi, G. G. Nair, and S. K. Prasad, J. Phys.: Condens. Matter **19**, 226213 (2007).